Electronic Research Archive

https://www.aimspress.com/journal/era

ERA, 34(5): 2732–2759.
DOI: 10.3934/era.2026125
Received: 12 February 2026
Revised: 21 March 2026
Accepted: 25 March 2026
Published: 30 March 2026

Research article

Dynamics of an emerging infectious disease with a behavior change and constrained treatment resources

Xinru Li, Ning Wang and Shengqiang Liu*

School of Mathematical Sciences, Tiangong University, Tianjin 300387, China

* **Correspondence:** Email: sqliu@tiangong.edu.cn.

Abstract: At the early stage of an emerging infectious disease outbreak, the interplay between individual protective behavior and therapeutic resources profoundly influences the effectiveness of epidemic control. By extending the classic behavior–disease coupling framework, this paper developed a dynamic model that concurrently incorporates heterogeneous behavioral adoption dynamics and saturation effects in treatment resources. Two behavioral regulation parameters were introduced to quantify their synergistic influence on transmission dynamics. Theoretical analysis yielded the basic reproduction number for both homogeneous and mixed systems, thereby establishing the threshold dynamics of the model. Numerical simulations demonstrated that increasing the intensity of behavioral adoption significantly reduces both the infection scale and transmission risk, and can even lower $\mathcal{R}_0$ below the epidemic. However, if the driving force for adoption is insufficient, transmission risk in the mixed system may exceed that in a system with no behavioral adoption, suggesting that ineffective interventions could exacerbate disease spread. Under resource constraints, our results indicate that large-scale, high-compliance behavioral interventions are essential for epidemic control. They further provides a mathematical basis for designing integrated strategies that balance "behavioral maintenance" and "resource allocation".

Keywords: emerging infectious diseases; behavioral-disease coupling model; resource constraints; basic reproduction number

1. Introduction

Infectious diseases continue to pose a significant global health challenge, accounting for more than 15 million deaths each year—representing over one-quarter of the worldwide mortality [1]. Emerging infectious diseases (EIDs), defined as infections newly appearing or rapidly increasing in incidence or geographic range [1] , include dengue fever, Influenza A (H1N1), Crimean-Congo hemorrhagic fever (CCHF), acute hepatitis in children, severe acute respiratory syndrome (SARS),

and COVID-19. Such EIDs not only threaten public health but also impose significant economic burdens worldwide [2–5], underscoring the critical need to study their disease transmission dynamics for guiding effective intervention strategies [6–8].

In response to emerging infectious diseases, non-pharmaceutical interventions (NPIs) — such as social distancing, mask-wearing, hand hygiene, risk communication, and isolation — have been widely adopted worldwide; pharmaceutical measures, e.g. , vaccination — have also been implemented where available [9]. However, the sudden onset of outbreaks often leads to insufficient emergency preparedness, triggering a strain on medical resources and thereby constraining overall control efficacy [10–15]. More complexly, disease transmission and human behavior form a tightly coupled feedback system: behavioral norms at the population level influence individual decision-making, individual protective behaviors in turn modulate viral transmission efficiency, and changes in epidemic dynamics reshape public risk perception and behavioral choices [16, 17]. Therefore, integrating insights from behavioral science with epidemiological dynamic modeling to construct behavior–disease coupled models has become a key research direction for deeply understanding and predicting epidemic progression [18, 19].

Mathematical modeling is a fundamental tool for studying infectious disease transmission and control. Since Kermack and McKendrick's foundational compartmental model in 1927, the field has advanced considerably [20, 21]. Recent research focuses increasingly on how behavioral change influences epidemic dynamics, making the integration of behavioral science into epidemiological models a major direction in modern epidemiology [22–24].

Existing models of behavioral transition can be categorized into two classes based on their formulation of transition mechanisms. The first class treats transition rates as dynamic processes rooted in behavioral theories [25–29]. For example, Ryan et al. incorporated the health belief model into an SIRS framework, showing that social influence and perceived threat drive protective behavior adoption and affect the basic reproduction number [27]. Their later work extended to testing and isolation behaviors, revealing how behavioral feedback creates discrepancies between reported and actual infections [28]. Similarly, Kaur et al. proposed a fear-disease coupling model, defining behavioral transition as a asocial contagion process dependent on infected and fearful individuals [29]. The second class employs constant transition rates to model behavioral state changes, emphasizing the structural impact of behavioral factors. Agaba et al. developed an SIRS model with constant rates distinguishing "private" and "public" awareness, showing that awareness spread can raise the epidemic threshold and reduce the final outbreak size [30]. However, this assumption limits capturing adaptive decision-making based on real-time epidemic risk. Shang et al. similarly used constant rates to describe movement between subgroups in a two-group SI model [31].

In summary, both approaches highlight the essential structural role of behavior in epidemic dynamics. Incorporating feedback from behavior to disease progression improves model representation of real-world interventions, guiding development of more explanatory and policy-relevant epidemiological models.

Although significant progress has been made in behavior-disease coupled modeling, a key limitation remains: most existing models do not adequately incorporate the realistic constraint of limited therapeutic resources, nor systematically examine behavioral dynamics within resource-constrained disease models. During the initial outbreak of an emerging infectious disease, the scarcity of treatment resources, including hospital beds, specific medications, and healthcare personnel, may interact with

the adoption or abandonment of individual protective behaviors in complex synergistic or antagonistic ways, jointly shaping the transmission trajectory and control outcomes. Therefore, constructing a unified mathematical modeling framework that simultaneously integrates dynamic transitions in behavioral heterogeneity and saturation effects of treatment resources to systematically investigate their synergistic regulatory mechanisms on infectious disease spread holds significant theoretical value and practical importance for improving targeted intervention strategies in public health emergencies.

To address this gap, we develop an epidemic dynamics model that simultaneously incorporates behavioral transition mechanisms and treatment resource saturation effects. Building on Ryan et al. [27], we stratify the population into two groups—those who adopt protective behaviors and those who do not, and incorporate a health belief model–based behavioral transition process plus a resource-dependent treatment saturation function. Unlike prior studies, this work specifically integrates a resource-dependent treatment saturation function to investigate the potential for optimizing epidemic control by modulating behavioral transition parameters under resource constraints. Theoretically, we derive and compare the basic reproduction numbers for mixed-behavior and homogeneous-behavior systems, establishing the associated threshold dynamics. Through numerical simulations, we further reveal how key parameters—including behavioral transition rates and social influence factors—collectively shape transmission risk and final epidemic scale in resource-limited settings. The results show that increasing behavioral adoption intensity markedly reduces infection size and transmission risk, and — under resource constraints — can lower the reproduction number below the epidemic threshold. Conversely, insufficient behavioral adoption (e.g., when ρ_1 is too small) may lead the mixed-behavior system to exhibit higher transmission risk than a system with no behavioral adoption, suggesting that incomplete or ineffective behavioral interventions could exacerbate epidemic spread. This study indicates that implementing large-scale, high-compliance behavioral interventions is critical for effective epidemic control under resource-limited conditions, and provides a mathematical foundation for designing integrated strategies that balance behavioral maintenance and resource allocation.

The paper is structured as follows. Section 2 presents the formulation of an infectious disease dynamic model that incorporates heterogeneous behavioral transitions and the saturation effect of treatment resources. Section 3 details the main theoretical findings, including the derivation of the basic reproduction numbers for both homogeneous and mixed systems. In Section 4, numerical simulations are conducted to investigate the impact of individual protective behavior adoption and limited treatment resources on disease transmission and control. Finally, Section 5 provides a summary and discussion of the study.

2. Model formulation

Building upon the behavior and disease (BaD) coupling model proposed by Ryan et al. [27], this study constructs an extended BaD dynamic model by incorporating the saturation effect of treatment resources. The model aims to characterise how the dynamic evolution of protective behaviors within a population influences the trajectory of infectious disease spread under resource-constrained conditions. The model construction follows the logical steps outlined below.

This study constructs an infectious disease dynamic model that incorporates behavioral dynamics and resource constraints, based on the following fundamental assumptions:

First, we consider a closed and homogeneously mixed population, ignoring migration and natural birth-death processes. This assumption implies that the total population size remains constant. We therefore normalize the total population to 1, so that each compartment variable (S_N, I_N, R_N, S_B, I_B, R_B) represents the proportion of the total population in that state. Consequently, we have the conservation relation $S_N + I_N + R_N + S_B + I_B + R_B = 1$. Disease transmission follows the classic SIRS (Susceptible–Infected–Recovered–Susceptible) framework, assuming that immunity acquired after recovery is only temporary. Individuals may voluntarily adopt protective behaviors, which effectively reduce their infection risk during contact. The dynamics of behavior adoption and abandonment are driven by the health belief model, with transition rates depending on individual risk perception, social influence, and other factors.

Furthermore, to capture the reality of strained treatment resources during the early stages of an emerging infectious disease, the model introduces resource constraints. Let the total available resources in the system be M ($0 \leq M \leq 1$), with a proportion m ($0 \leq m \leq M$) allocated to the non-behavior-adopting group and the remaining $M-m$ allocated to the behavior-adopting group, so as to examine the impact of different resource allocation strategies. At the same time, the model incorporates a treatment saturation function to reflect the saturation effect that occurs when medical resources approach or reach their upper limit, thereby providing a more realistic simulation of disease transmission dynamics under resource constraints. Epidemiologically, this function represents the limitation of healthcare resources: as the infected population grows, the per-capita treatment efficiency declines due to constraints such as finite hospital capacity, limited medical staff, and inadequate supplies.

$$
\begin{aligned}
\frac{dS_N(t)}{dt} &= -\lambda(t)S_N(t) + \nu R_N(t) - \omega(t)S_N(t) + \alpha(t)S_B(t),\\
\frac{dI_N(t)}{dt} &= \lambda(t)S_N(t) - \gamma_a I_N(t) - \frac{\gamma_t\, m I_N(t)}{1+I_N(t)} - \omega(t)I_N(t) + \alpha(t)I_B(t),\\
\frac{dR_N(t)}{dt} &= \gamma_a I_N(t) + \frac{\gamma_t\, m I_N(t)}{1+I_N(t)} - \nu R_N(t) - \omega(t)R_N(t) + \alpha(t)R_B(t),\\
\frac{dS_B(t)}{dt} &= -q\lambda(t)S_B(t) + \nu R_B(t) + \omega(t)S_N(t) - \alpha(t)S_B(t),\\
\frac{dI_B(t)}{dt} &= q\lambda(t)S_B(t) - \gamma_a I_B(t) - \frac{\gamma_t\,(M-m) I_B(t)}{1+I_B(t)} + \omega(t)I_N(t) - \alpha(t)I_B(t),\\
\frac{dR_B(t)}{dt} &= \gamma_a I_B(t) + \frac{\gamma_t\,(M-m) I_B(t)}{1+I_B(t)} - \nu R_B(t) + \omega(t)R_N(t) - \alpha(t)R_B(t).
\end{aligned}
\tag{2.1}
$$

The framework is mathematically captured by the system of ordinary differential equations (ODEs) given above, with its compartmental structure depicted in the flowchart of Figure 1.

To simultaneously characterize epidemiological and behavioral states, a stratified compartmental modeling approach is employed. Each epidemiological state ($X \in \{S, I, R\}$) is further subdivided into two compartments: those not adopting protective behaviors (X_N) and those adopting protective behaviors (X_B). It is noteworthy that although recovered individuals (R) possess immunity to infection, their behavioral state still participates in the feedback loop of behavioral dynamics through social influence mechanisms. Consequently, they are also incorporated into the hierarchical structure. The total population satisfies $S_N + I_N + R_N + S_B + I_B + R_B = 1$.

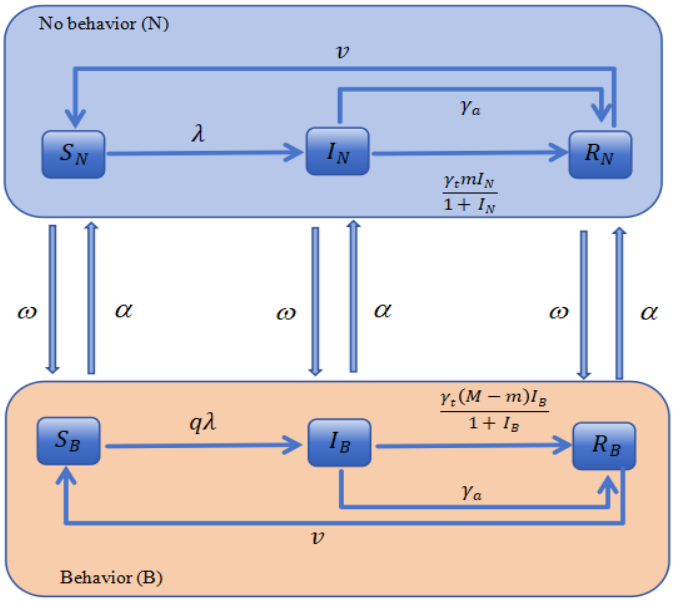

Figure 1. Schematic diagram of Model (2.1) capturing behavioral transition mechanisms and treatment resource saturation effects.

The coupled dynamics of the model are described by two sets of equations. Transitions between epidemiological states follow the standard SIRS framework, but the calculation of infectivity incorporates behavioral stratification: $\lambda(t) = \beta[I_N(t) + \sigma I_B(t)]$, where β denotes the transmission rate, and σ represents the protective efficacy of behaviors against infectiousness. Transitions between behavioral states occur within each epidemiological compartment, governed by the behavioral adoption rate $\omega(t)$ and the behavioral abandonment rate $\alpha(t)$. We assume that behavioral transition rates are independent of the specific epidemiological state an individual occupies, meaning that behavioral change is primarily driven by universal psychosocial factors.

The behavioral conversion rates $\omega(t)$ and $\alpha(t)$ are quantified based on the health belief model. Referencing the parametric form by Ryan et al. [28], they are defined as

$$\omega(t) = \rho_1(\omega_1 B(t) + \omega_2 I(t) + \omega_3),$$
$$\alpha(t) = \rho_2(\alpha_1 N(t) + \alpha_2),$$

where $B(t)$ and $N(t)$ denote the proportions of the population adopting and not adopting protective behaviors, respectively, and let $I(t)$ represent the total infection prevalence. The parameter ω_1 models the social contagion effect that drives behavior adoption, ω_2 governs the adoption rate in response to perceived disease threat (often linked to fear or risk perception), and ω_3 accounts for spontaneous (baseline) adoption. Conversely, α_1 captures the social spread of behavior abandonment, while α_2 represents spontaneous abandonment. Building on this formulation, the present study introduces two key modulation parameters, ρ_1 and ρ_2, to scale the overall rates of behavior adoption and abandonment, respectively. This extension allows flexible simulation of behavioral transition intensity under varying intervention strengths and supports subsequent analysis of optimized control strategies.

In summary, this model forms a closed-loop "perception–behavior–disease" feedback system by coupling epidemiological dynamics with theory-based behavioral transition dynamics, incorporating

a treatment resource saturation function. This framework dynamically simulates the complex interactions between population protective behaviors and infectious disease transmission under resource constraints, providing a quantitative analytical tool for evaluating and optimizing non-pharmaceutical intervention strategies targeting behavioral change.

Table 1. Descriptions and values of parameters involved in Model (2.1).

Parameter	Description	Value	Units	Reference
β	Transmission rate of infected individuals	0.2	day^{-1}	Assumed
σ	Reduction in infectiousness due to protective behavior	0.5	–	[27]
q	Reduction in susceptibility due to protective behavior	0.5	–	[27]
γ_a	Natural recovery rate	0.034	day^{-1}	Assumed
γ_t	Recovery rate due to treatment	0.047	day^{-1}	Assumed
M	Maximum available treatment resources (proportion)	0.05	–	Assumed
m	Proportion of treatment resources allocated to non-behaving group	0.02	–	Assumed
ν	The rate of waning immunity	0.025	day^{-1}	[28]
ρ_1	Overall control parameter for taking actions	1	–	Assumed
ρ_2	Overall control parameter for abandonment behavior	1	–	Assumed
ω_1	Social transmission rate of protective behavior	0.4	day^{-1}	[27]
ω_2	Rate of behavior adoption in response to perceived illness threat	7	day^{-1}	[28]
ω_3	Spontaneous (baseline) adoption rate of protective behavior	0.2	day^{-1}	[27]
α_1	Social transmission rate of behavior abandonment	0.2	day^{-1}	[9]
α_2	Spontaneous (baseline) abandonment rate of protective behavior	0.1	day^{-1}	[9]

3. Threshold analysis

This section first examines the dynamical properties of two single-system models derived from the full Model (2.1): a SIRS model without protective behavior (Model (3.1)), and a protective-behavior SIRS model with universal adoption (Model (3.6)). The two models differ only in their susceptibility and infectiousness parameters. For each, we analyze the system stability, basic reproduction number, existence and stability of equilibria, and persistence. For the mixed system, where protected and unprotected individuals coexist and can switch states, we focus on the basic reproduction number, the existence of disease-free equilibria, and their local asymptotic stability.

3.1. Non-behavioral system

As a baseline scenario, we consider the case where protective behaviors are not adopted and therapeutic resources are constrained. In this situation, the model simplifies to a classical SIRS model without behavioral dynamics, governed by the following system:

$$\begin{aligned} \frac{\mathrm{d}S_N}{\mathrm{d}t} &= -\beta S_N I_N + \nu R_N, \\ \frac{\mathrm{d}I_N}{\mathrm{d}t} &= \beta S_N I_N - \gamma_a I_N - \frac{\gamma_t M I_N}{1 + I_N}, \\ \frac{\mathrm{d}R_N}{\mathrm{d}t} &= \gamma_a I_N + \frac{\gamma_t M I_N}{1 + I_N} - \nu R_N. \end{aligned} \tag{3.1}$$

3.1.1. Disease-free equilibrium and basic reproduction number

This subsection derives the disease-free equilibrium (DFE), calculates the basic reproduction number $\mathcal{R}_{0,1}$ using the next-generation matrix (NGM) method [32], and analyses the local stability of the DFE.

Model (3.1) admits a DFE given by $E_{0,1} = (1, 0, 0)$. Following the NGM framework, we define the infection rate vector $\mathcal{F}$ and the transition rate vector $\mathcal{V}$ for the infected compartment I_N as

$$\mathcal{F}(I_N) = \beta I_N S_N, \qquad \mathcal{V}(I_N) = \gamma_a I_N + \frac{\gamma_t M I_N}{1 + I_N}.$$

Linearizing these terms at $E_{0,1}$ yields the matrices

$$F = \left.\frac{\partial \mathcal{F}}{\partial I_N}\right|_{E_{0,1}} = \beta, \quad V = \left.\frac{\partial \mathcal{V}}{\partial I_N}\right|_{E_{0,1}} = \gamma_a + \gamma_t M.$$

The basic reproduction number, defined as the spectral radius of the next-generation matrix FV^{-1}, is therefore

$$\mathcal{R}_{0,1} = \frac{\beta}{\gamma_a + \gamma_t M}$$

which corresponds to the basic reproduction number for the homogeneous system without protective behavior, representing the average number of secondary infections generated by a single infectious individual in a fully susceptible population when no behavioral interventions are in place [33].

Theorem 3.1. *The DFE $E_{0,1}$ of Model (3.1) is locally asymptotically stable if $\mathcal{R}_{0,1} < 1$, and unstable if $\mathcal{R}_{0,1} > 1$.*

Proof. Using the conservation relation $S_N + I_N + R_N = 1$, Model (3.1) can be reduced to a two-dimensional system in the variables S_N and I_N:

$$\begin{aligned} \frac{\mathrm{d}S_N}{\mathrm{d}t} &= -\beta S_N I_N + \nu(1 - S_N - I_N), \\ \frac{\mathrm{d}I_N}{\mathrm{d}t} &= \beta S_N I_N - \gamma_a I_N - \frac{\gamma_t M I_N}{1 + I_N}. \end{aligned} \tag{3.2}$$

The Jacobian matrix of (3.2) evaluated at $E_{0,1} = (1, 0)$ is

$$J(E_{0,1}) = \begin{pmatrix} -\nu & -\beta - \nu \\ 0 & \beta - (\gamma_a + \gamma_t M) \end{pmatrix}.$$

The characteristic equation $(\lambda + \nu)(\lambda - [\beta - (\gamma_a + \gamma_t M)]) = 0$ yields the eigenvalues $\lambda_1 = -\nu$ and $\lambda_2 = \beta - (\gamma_a + \gamma_t M)$. Since $\lambda_1 = -\nu < 0$ is always negative, the stability of the equilibrium is determined solely by the sign of λ_2. The condition $\lambda_2 < 0$ holds if and only if $\beta < \gamma_a + \gamma_t M$, which is equivalent to $\mathcal{R}_{0,1} < 1$.

Hence, both eigenvalues have negative real parts if and only if $\mathcal{R}_{0,1} < 1$, implying that $E_{0,1}$ is locally asymptotically stable. Conversely, if $\mathcal{R}_{0,1} > 1$, then $\lambda_2 > 0$ and $E_{0,1}$ is unstable.

While Theorem 3.1 establishes the local asymptotic stability of the DFE, it does not guarantee global convergence under the same condition. To address the long-term behavior of the system for all initial conditions within the feasible region, we now present a global stability result. This requires a stronger condition, as stated in the following theorem.

Theorem 3.2. *The DFE $E_{0,1}$ of Model (3.1) is globally asymptotically stable in the feasible region $\Omega = \left\{(S_N, I_N, R_N) \in \mathbb{R}^3_+ : S_N + I_N + R_N = 1\right\}$ if $\beta - \gamma_a - \frac{\gamma_t M}{2} \leq 0$ (equivalent to $\mathcal{R}_{0,1} \leq 1 - \frac{\gamma_t M}{2(\gamma_a + \gamma_t M)}$).*

Proof. We prove global asymptotic stability by constructing a suitable Lyapunov function [34, 35]. Define

$$V(S_N, I_N) = S_N - 1 - \ln S_N + I_N,$$

where V is defined on the region $\{S_N > 0, I_N \geq 0, S_N + I_N \leq 1\}$, and $V(1, 0) = 0$, $V(S_N, I_N) > 0$ for $(S_N, I_N) \neq (1, 0)$. Note that $V(1, 0) = 0$ and $V(S_N, I_N) > 0$ for all $(S_N, I_N) \neq (1, 0)$ in the domain $S_N > 0, I_N \geq 0$. Differentiating V along the trajectories of the reduced Model (3.2) gives

$$\begin{aligned} \frac{dV}{dt} &= \left(1 - \frac{1}{S_N}\right)\frac{dS_N}{dt} + \frac{dI_N}{dt} \\ &= \left(1 - \frac{1}{S_N}\right)[-\beta S_N I_N + \nu(1 - S_N - I_N)] + \beta S_N I_N - \gamma_a I_N - \frac{\gamma_t M I_N}{1 + I_N}. \end{aligned}$$

Expanding and simplifying, we obtain

$$\begin{aligned} \frac{dV}{dt} &= -\beta S_N I_N + \nu(1 - S_N - I_N) + \beta I_N - \frac{\nu(1 - S_N - I_N)}{S_N} \\ &\quad + \beta S_N I_N - \gamma_a I_N - \frac{\gamma_t M I_N}{1 + I_N} \\ &= \nu(1 - S_N - I_N)\left(1 - \frac{1}{S_N}\right) + \beta I_N - \gamma_a I_N - \frac{\gamma_t M I_N}{1 + I_N}. \end{aligned}$$

Since $R_N = 1 - S_N - I_N \geq 0$ and $1 - 1/S_N \leq 0$ (because $S_N \leq 1$ in the feasible region), the first term $\nu R_N(1 - 1/S_N)$ is non-positive. Consequently,

$$\frac{dV}{dt} \leq \beta I_N - \gamma_a I_N - \frac{\gamma_t M I_N}{1 + I_N} \leq \beta I_N - \gamma_a I_N - \frac{\gamma_t M I_N}{2} = \left(\beta - \gamma_a - \frac{\gamma_t M}{2}\right) I_N.$$

Whenever $\mathcal{R}_{0,1} \leq 1 - \frac{\gamma_t M}{2(\gamma_a+\gamma_t M)}$, the derivative of the Lyapunov function satisfies $\frac{dV}{dt} \leq 0$ for all $I_N > 0$, with $\frac{dV}{dt} = 0$ holding only at $I_N = 0$. It follows that the largest invariant set is contained in the set where $I_N = 0$. In the subsystem with $I_N = 0$, from Model (3.1) we obtain $\frac{dS_N}{dt} = \nu R_N$ and $\frac{dR_N}{dt} = -\nu R_N$. Combined with $S_N + R_N = 1$, it is easy to see that the invariant set contains only $E_{0,1}$. Thus, an application of LaSalle's invariance principle [36] establishes the global asymptotic stability of $E_{0,1}$ under this parameter condition.

3.1.2. Endemic equilibrium and its stability

Having established the existence and stability of the disease-free equilibrium, we now examine the endemic equilibrium of Model (3.1), which corresponds to a state where the disease persists. This subsection derives the conditions for the existence of this equilibrium and analyzes its local stability.

Let $E^*_{0,1} = (S^*_N, I^*_N, R^*_N)$ represent a nontrivial (endemic) equilibrium. Setting the time derivatives in (3.1) to zero and applying the population conservation relation $S_N + I_N + R_N = 1$ yields the following two equations for S_N:

$$S_N = \frac{\nu(1 - I_N)}{\beta I_N + \nu}, \tag{3.3}$$

$$S_N = \frac{\gamma_a}{\beta} + \frac{\gamma_t M}{\beta(1 + I_N)}. \tag{3.4}$$

Equating the right-hand sides of (3.3) and (3.4) results in a quadratic equation for the infected proportion I_N: $aI_N^2 + bI_N + c = 0$, with coefficients

$$a = \beta(\nu + \gamma_a) > 0, \qquad b = \gamma_a(\beta + \nu) + \beta\gamma_t M > 0, \qquad c = \nu(\gamma_a + \gamma_t M - \beta).$$

Notably, c can be expressed in terms of the basic reproduction number $\mathcal{R}_{0,1} = \beta/(\gamma_a + \gamma_t M)$ as $c = \nu(\gamma_a + \gamma_t M)(1 - \mathcal{R}_{0,1})$. Thus, the sign of c is entirely determined by $\mathcal{R}_{0,1}$: $c > 0$ when $\mathcal{R}_{0,1} < 1$, and $c < 0$ when $\mathcal{R}_{0,1} > 1$. Define the quadratic function $F(I_N) = aI_N^2 + bI_N + c$. Evaluating F at the boundaries of the biologically feasible interval $I_N \in [0, 1]$ gives

$$F(0) = c, \qquad F(1) = a + b + c = 2\gamma_a(\beta + \nu) + \beta\gamma_t M + \nu\gamma_t M > 0.$$

If $\mathcal{R}_{0,1} > 1$, then $c < 0$ and consequently $F(0) < 0 < F(1)$. By the intermediate value theorem, there exists at least one root $I^*_N \in (0, 1)$. Moreover, since $a > 0$, the quadratic function F is strictly convex, which guarantees the uniqueness of this root within $(0, 1)$. Therefore, a unique endemic equilibrium exists if and only if $\mathcal{R}_{0,1} > 1$. For $\mathcal{R}_{0,1} \leq 1$, no endemic equilibrium exists, and the disease-free equilibrium remains the only steady state.

We now establish the local stability of the endemic equilibrium when it exists.

Theorem 3.3. *If $\mathcal{R}_{0,1} > 1$, then the unique endemic equilibrium $E^*_{0,1}$ of Model (3.1) is locally asymptotically stable.*

Proof. To analyze stability, we consider the Jacobian matrix of Model (3.1) evaluated at $E^*_{0,1}$:

$$J(E_{0,1}^*) = \begin{pmatrix} -\beta I_N^* - \nu & -\beta S_N^* - \nu \\ \beta I_N^* & \beta S_N^* - \gamma_a - \dfrac{\gamma_t M}{(1+I_N^*)^2} \end{pmatrix}.$$

Local asymptotic stability requires that both eigenvalues of $J(E_{0,1}^*)$ have negative real parts, which is equivalent to the conditions $\mathrm{Tr}(J) < 0$ and $\mathrm{Det}(J) > 0$ for a two-dimensional system.

The trace and determinant are

$$\mathrm{Tr}(J(E_{0,1}^*)) = -\beta I_N^* - \nu + \beta S_N^* - \gamma_a - \frac{\gamma_t M}{(1+I_N^*)^2},$$

$$\mathrm{Det}(J(E_{0,1}^*)) = (-\beta I_N^* - \nu)\Big(\beta S_N^* - \gamma_a - \frac{\gamma_t M}{(1+I_N^*)^2}\Big) + (\beta S_N^* + \nu)\beta I_N^*.$$

After detailed algebraic manipulation, we derive two stability thresholds, $\mathcal{T}_1$ and $\mathcal{T}_2$, such that: $\mathrm{Det}(J) > 0$ if and only if $\mathcal{R}_{0,1} > \mathcal{T}_1$ and $\mathrm{Tr}(J) < 0$ if and only if $\mathcal{R}_{0,1} > \mathcal{T}_2$.

The explicit forms of these thresholds are

$$\mathcal{T}_1 = \frac{\gamma_t M \nu}{(\gamma_a + \gamma_t M)((1+I_N^*)^2(\gamma_a+\nu) + \gamma_t M)},$$
$$\mathcal{T}_2 = \frac{\gamma_t M((1+I_N^*) - \nu((1+I_N^*)^2 - \gamma_t M))}{I_N^*(\gamma_a + \gamma_t M)(1+I_N^*)^2}.$$

Therefore, the endemic equilibrium is locally asymptotically stable when

$$\mathcal{R}_{0,1} > \max\{\mathcal{T}_1,\ \mathcal{T}_2,\ 1\}, \tag{3.5}$$

where the condition $\mathcal{R}_{0,1} > 1$ ensures the equilibrium's existence.

We now prove that both $\mathcal{T}_1$ and $\mathcal{T}_2$ are strictly less than 1. For $\mathcal{T}_1$, consider the numerator inequality

$$\begin{aligned} &\gamma_a M\nu - (\gamma_a + \gamma_t M)((1+I_N^*)^2(\gamma_a+\nu) + \gamma_t M) \\ &= -(\gamma_a + \gamma_t M)[(I_N^{*2} + 2I_N^*)\gamma_a + \gamma_t M] - \gamma_a(\gamma_a + \nu + \gamma_t M) - \gamma_t M(\gamma_a + \gamma_t M) < 0. \end{aligned}$$

Since the denominator of $\mathcal{T}_1$ is positive, this implies $\mathcal{T}_1 < 1$. For $\mathcal{T}_2$, we have

$$\begin{aligned} &\gamma_t M((1+I_N^*) - \nu((1+I_N^*)^2 - \gamma_t M)) - I_N^*(\gamma_a + \gamma_t M)(1+I_N^*)^2 \\ &= -\nu(1+I_N^*)^2 - \gamma_a(I_N^* + 2I_N^{*2} + I_N^{*3}) - \gamma_t M(2I_N^{*2} + I_N^{*3}) < 0. \end{aligned}$$

Given that the denominator of $\mathcal{T}_2$ is positive, we conclude $\mathcal{T}_2 < 1$.

Consequently, $\max\{\mathcal{T}_1, \mathcal{T}_2, 1\} = 1$. Condition (3.5) thus simplifies to $\mathcal{R}_{0,1} > 1$, which is precisely the condition for the existence of the endemic equilibrium. Therefore, whenever $E_{0,1}^*$ exists, it is locally asymptotically stable.

3.1.3. Uniform persistence of the disease

Theorem 3.4. *If $\mathcal{R}_{0,1} > 1$, then Model (3.1) is uniformly persistent. Specifically, there exists a constant $\varepsilon > 0$ such that for any initial condition satisfying $I_N(0) > 0$, the solution satisfies* $\liminf_{t\to\infty} I_N(t) \geq \varepsilon$.

Proof. Define the phase space

$$X = \{(S_N, I_N, R_N) \in \mathbb{R}^3_+ : S_N + I_N + R_N = 1\},$$

and its subsets

$$X_1 = \{(S_N, I_N, R_N) \in X : I_N > 0\}, \quad X_2 = \{(S_N, I_N, R_N) \in X : I_N = 0\}.$$

It is straightforward to verify that both X_1 and X_2 are positively invariant under the flow of Model (3.1). In particular, if $I_N(0) = 0$, then we have $I_N(t) \equiv 0$; if $I_N(0) > 0$, then $I_N(t) > 0$ for all $t > 0$.

On X_2, the system reduces to

$$\frac{dR_N}{dt} = -\nu R_N, \quad S_N = 1 - R_N.$$

Solving this yields $R_N(t) = R_N(0)e^{-\nu t}$. Hence, as $t \to \infty$, we have $R_N(t) \to 0$ and consequently $S_N(t) \to 1$. Therefore, all trajectories in X_2 converge to the disease-free equilibrium (DFE) $E_{0,1} = (1, 0, 0)$, which is a global attractor in X_2.

The Jacobian matrix of the system at $E_{0,1}$ has one eigenvalue equal to $\beta - \gamma_a - \gamma_t M$. Since $\mathcal{R}_{0,1} > 1$ implies $\beta > \gamma_a + \gamma_t M$, this eigenvalue is positive. Thus, $E_{0,1}$ is a saddle point: it is stable within X_2 but unstable in the direction transverse to X_2 (i.e., into X_1).

We argue by contradiction. Suppose there exists an initial point $x \in X_1$ such that the corresponding solution satisfies

$$\lim_{t\to\infty}(S_N(t), I_N(t), R_N(t)) = (1, 0, 0).$$

Then, for any sufficiently small $\epsilon \geq 0$, there exists $T > 0$ such that for all $t > T$, $S_N(t) > 1 - \epsilon, \quad 0 < I_N(t) < \epsilon$. Now consider the equation for I_N:

$$\frac{dI_N}{dt} = \beta S_N I_N - \gamma_a I_N - \frac{\gamma_t M I_N}{1 + I_N}.$$

Since $1/(1 + I_N) \leq 1$, we have the lower bound

$$\frac{dI_N}{dt} \geq \beta S_N I_N - \gamma_a I_N - \gamma_t M I_N = I_N(\beta S_N - \gamma_a - \gamma_t M).$$

Because $R_{0,1} > 1$, we can choose ϵ small enough so that $\beta(1 - \epsilon) - \gamma_a - \gamma_t M > 0$. Let $c = \beta(1 - \epsilon) - \gamma_a - \gamma_t M > 0$. Then for $t > T$, $\frac{dI_N}{dt} \geq cI_N$, which implies $I_N(t) \geq I_N(T)e^{c(t-T)}$. Hence, $I_N(t)$ grows exponentially, contradicting the assumption that $I_N(t) \to 0$. Therefore, no trajectory starting in X_1 can converge to $E_{0,1}$.

Since $E_{0,1}$ is a global attractor in X_2 and no trajectory from X_1 tends to $E_{0,1}$, then, there exists $\epsilon > 0$ such that for any initial condition in X_1,

$$\liminf_{t\to\infty} I_N(t) \geq \epsilon.$$

Moreover, by the conservation of total population, S_N and R_N also have positive lower bounds in the limit. This completes the proof.

3.2. Complete behavioral system

In contrast to the non-behavioral system analyzed in the previous subsection, we now examine the scenario where all individuals consistently adopt protective behaviors, while treatment resources remain limited. The dynamics of this complete behavioral system are governed by the following equations:

$$\begin{aligned} \frac{\mathrm{d}S_B}{\mathrm{d}t} &= -q\beta\sigma S_B I_B + \nu R_B, \\ \frac{\mathrm{d}I_B}{\mathrm{d}t} &= q\beta\sigma S_B I_B - \gamma_a I_B - \frac{\gamma_t M I_B}{1+I_B}, \\ \frac{\mathrm{d}R_B}{\mathrm{d}t} &= \gamma_a I_B + \frac{\gamma_t M I_B}{1+I_B} - \nu R_B. \end{aligned} \tag{3.6}$$

The structure of Model (3.6) is analogous to that of the non-behavioral Model (3.1), with the key difference being the inclusion of the behavioral factors q and σ in the transmission term. Consequently, the analytical approach and stability results follow a similar pattern. For brevity, we present only the main results below; detailed derivations are omitted as they parallel those in Section 3.1.2.

The basic reproduction number for the complete behavioral system is given by

$$\mathcal{R}_{0,2} = \frac{q\sigma\beta}{\gamma_a + \gamma_t M},$$

which corresponds to the basic reproduction number for the homogeneous system with universal protective behavior, reflecting the transmission potential when everyone adopts effective protective measures [33].

Theorem 3.5 (DFE stability)**.** *The disease-free equilibrium $E_{0,2} = (1, 0, 0)$ of Model (3.6) is locally asymptotically stable if $\mathcal{R}_{0,2} < 1$, and unstable if $\mathcal{R}_{0,2} > 1$.*

Theorem 3.6 (Endemic equilibrium stability)**.** *If $\mathcal{R}_{0,2} > 1$, the unique endemic equilibrium $E^*_{0,2}$ of Model (3.6) is locally asymptotically stable.*

Analogous to the persistence result Theorem 3.4 for the non-behavioral system (3.1), we establish the following uniform persistence result for Model (3.6).

Theorem 3.7 (Disease persistence)**.** *If $\mathcal{R}_{0,2} > 1$, then Model (3.6) is uniformly persistent. Specifically, there exists a constant $\varepsilon > 0$ such that for any initial condition satisfying $I_B(0) > 0$, the solution satisfies $\liminf_{t\to\infty} I_B(t) \geq \varepsilon$.*

Remark 3.8. *These results collectively indicate that when protective behaviors are universally adopted, the threshold condition for disease invasion and persistence is modified by the product $q\sigma$, reflecting the combined effect of reduced susceptibility and reduced infectiousness.*

3.3. Heterogeneous population system

This section analyzes the full mixed system, in which individuals with and without protective behavior coexist. We introduce three distinct reproduction numbers: the behavioral reproduction number $\mathcal{R}_0^B$, the disease reproduction number $\mathcal{R}_0^D$, and the coupled basic reproduction number $\mathcal{R}_0$. Their respective threshold conditions decouple the behavioral and infection dynamics in isolation, as well as capture their full interaction. We then analyze the existence and stability of the disease-free equilibrium for the mixed system.

3.3.1. Threshold conditions

We first define three key threshold quantities, two of which decouple the behavioral and infection dynamics, while the third reflects their joint effect.

Disease reproduction number. When behavioral dynamics are absent (i.e., $\alpha = \omega = 0$), the mixed BaD SIRS model reduces to the classical SIRS model. In this case, the infection threshold is given by the basic reproduction number:

$$\mathcal{R}_0^D = \frac{\beta}{\gamma_a + \gamma_t M}.$$

In epidemiological terms, when in the absence of behavioral interventions, $\mathcal{R}_0^D$ represents the average number of secondary infections caused by a single infected individual within a fully susceptible population.

Behavioral reproduction number. Conversely, in the absence of infection ($I = 0$), the evolution of the proportion of individuals adopting protective behavior, B, is governed by $\dot{B} = (\rho_1\omega_1 B + \rho_1\omega_3)N - (\rho_2\alpha_1 N + \rho_2\alpha_2)B$, where $N = 1 - B$ denotes the proportion of non-behavers. Linearizing around $B = 0$ (i.e., $N = 1$) yields $\dot{B} = (\rho_1\omega_1 - (\rho_2\alpha_1 + \rho_2\alpha_2))B + \rho_1\omega_3$, whose solution is

$$B(t) = \left(B_0 + \frac{\rho_1\omega_3}{\rho_1\omega_1 - \rho_2(\alpha_1 + \alpha_2)}\right) e^{(\rho_1\omega_1 - \rho_2(\alpha_1+\alpha_2))t} - \frac{\rho_1\omega_3}{\rho_1\omega_1 - \rho_2(\alpha_1 + \alpha_2)}, \tag{3.7}$$

with $B_0 = B(0)$. Equation (3.7) shows that behavior will always emerge if $\omega_3 \neq 0$, but spreads as a genuine social contagion only when

$$\rho_1\omega_1 - \rho_2(\alpha_1 + \alpha_2) > 0.$$

This condition leads to the definition of the behavioral reproduction number

$$\mathcal{R}_0^B = \frac{\rho_1\omega_1}{\rho_2(\alpha_1 + \alpha_2)}.$$

The behavioral reproduction number quantifies the potential for protective behaviors to spread as a social contagion in the absence of infection.

Coupled basic reproduction number. Finally, we consider the full Model (2.1) with both disease transmission and behavioral dynamics. The infected compartments are I_N and I_B. Following the next-generation matrix (NGM) method [32], we define the vectors of new infection terms $\mathcal{F}$ and transition terms $\mathcal{V}$ as

$$\begin{pmatrix} \frac{\mathrm{d}I_N}{\mathrm{d}t} \\ \frac{\mathrm{d}I_B}{\mathrm{d}t} \end{pmatrix} = \mathcal{F}(I_N, I_B) - \mathcal{V}(I_N, I_B) = \begin{pmatrix} \beta(I_N + \sigma I_B)S_N \\ q\beta(I_N + \sigma I_B)S_B \end{pmatrix} - \begin{pmatrix} \gamma_a I_N + \frac{\gamma_t m I_N}{1 + I_N} + \omega I_N - \alpha I_B \\ \gamma_a I_B + \frac{\gamma_t (M - m) I_B}{1 + I_B} - \omega I_N + \alpha I_B \end{pmatrix}.$$

Linearizing around the disease-free equilibrium $E_0 = (S_N^*, 0, 0, S_B^*, 0, 0)$, we obtain the Jacobian matrices:

$$F = D\mathcal{F}(I_N, I_B)\big|_{E_0} = \begin{pmatrix} \beta S_N^* & \sigma\beta S_N^* \\ q\beta S_B^* & q\sigma\beta S_B^* \end{pmatrix},$$

$$V = D\mathcal{V}(I_N, I_B)\big|_{E_0} = \begin{pmatrix} \gamma_a + \gamma_t m + \omega_0 & -\alpha_0 \\ -\omega_0 & \gamma_a + \gamma_t(M-m) + \alpha_0 \end{pmatrix},$$

where $S_N^* + S_B^* = 1$, $\omega_0 = \rho_1(\omega_1 S_B^* + \omega_3)$, and $\alpha_0 = \rho_2(\alpha_1 S_N^* + \alpha_2)$. The next-generation matrix is $K = FV^{-1}$. After computing V^{-1} and the product FV^{-1}, we find

$$K = FV^{-1} = \begin{pmatrix} \dfrac{\beta S_N^*(\gamma_a + \gamma_t(M-m) + \alpha_0) + \beta\sigma S_N^*\omega_0}{\Delta} & \dfrac{\beta\sigma S_N^*(\gamma_a + \gamma_t m + \omega_0) + \beta S_N^*\alpha_0}{\Delta} \\ \dfrac{q\beta S_B^*(\gamma_a + \gamma_t(M-m) + \alpha_0) + q\beta\sigma S_B^*\omega_0}{\Delta} & \dfrac{q\beta\sigma S_B^*(\gamma_a + \gamma_t m + \omega_0) + q\beta S_B^*\alpha_0}{\Delta} \end{pmatrix},$$

with $\Delta = (\gamma_a + \gamma_t m + \omega_0)(\gamma_a + \gamma_t(M-m) + \alpha_0) - \alpha_0\omega_0$.

The basic reproduction number $\mathcal{R}_0$ is defined as the spectral radius of K. Solving the characteristic equation $\det(K - \lambda I) = 0$ yields the dominant eigenvalue. For the present structure of K, the spectral radius simplifies to

$$\mathcal{R}_0 = \frac{\beta S_N^*(\gamma_a + \gamma_t(M-m) + \alpha_0) + \beta\sigma S_N^*\omega_0}{\Delta} + \frac{q\beta\sigma S_B^*(\gamma_a + \gamma_t m + \omega_0) + q\beta S_B^*\alpha_0}{\Delta}. \tag{3.8}$$

This expression represents the average number of secondary infections generated by a single infectious case introduced into a completely susceptible population [33].

3.3.2. Existence of the disease-free equilibrium

A disease-free equilibrium (DFE) of the mixed system corresponds to a state in which infection is absent ($I_N^* = I_B^* = 0$) while protective behavior may be present ($B^* > 0$). Such an equilibrium can be written as $E_0 = (S_N^*, 0, 0, S_B^*, 0, 0) = (N^*, 0, 0, B^*, 0, 0)$, where $N^* = 1 - B^*$ and B^* is determined by the steady-state condition of the behavioral dynamics. Setting $\dot{B} = 0$ in the absence of infection yields the quadratic equation

$$(\rho_2\alpha_1 - \rho_1\omega_1)B^2 - (\rho_2\alpha_1 - \rho_1\omega_1 + \rho_1\omega_3 + \rho_2\alpha_2)B + \rho_1\omega_3 = 0.$$

Define the quadratic function

$$F(B) = (\rho_2\alpha_1 - \rho_1\omega_1)B^2 - (\rho_2\alpha_1 - \rho_1\omega_1 + \rho_1\omega_3 + \rho_2\alpha_2)B + \rho_1\omega_3.$$

Observing that $F(0) = \rho_1\omega_3 \geq 0$ and $F(1) = -\rho_2\alpha_2 \leq 0$, the intermediate value theorem guarantees the existence of at least one root $B^* \in (0, 1]$. Moreover, because F is quadratic, this root is unique within the interval.

Two special cases admit explicit solutions:

- If $\rho_2\alpha_1 = \rho_1\omega_1$, the equation becomes linear, giving

$$B^* = \frac{\rho_1\omega_3}{\rho_1\omega_3 + \rho_2\alpha_2}.$$

- For $\rho_2\alpha_1 \neq \rho_1\omega_1$, the unique admissible root is

$$B^* = \frac{\rho_2\alpha_1 - \rho_1\omega_1 + \rho_1\omega_3 + \rho_2\alpha_2 - \sqrt{(\rho_2\alpha_1 - \rho_1\omega_1 + \rho_1\omega_3 + \rho_2\alpha_2)^2 - 4(\rho_2\alpha_1 - \rho_1\omega_1)\rho_1\omega_3}}{2(\rho_2\alpha_1 - \rho_1\omega_1)}.$$

When spontaneous adoption is absent ($\omega_3 = 0$), the expression simplifies to

$$B^* = \frac{\rho_2(\alpha_1 + \alpha_2)}{2(\rho_2\alpha_1 - \rho_1\omega_1)}(1 - \mathcal{R}_0^B) - \left|1 - \mathcal{R}_0^B\right|,$$

which clearly highlights the dependence of the behavioral steady state on the behavioral reproduction number $\mathcal{R}_0^B$: $B^* = 0$ when $\mathcal{R}_0^B < 1$, and $B^* > 0$ when $\mathcal{R}_0^B > 1$. Thus, in the absence of exogenous adoption pressure, protective behavior can persist only if its reproduction number exceeds unity.

3.3.3. Stability of the disease-free equilibrium

Having established the existence and explicit form of the disease-free equilibrium (DFE), we now analyze its local asymptotic stability. The stability of the DFE is determined by the threshold condition on the basic reproduction number $\mathcal{R}_0$, which quantifies the potential for disease invasion in a fully susceptible population.

Theorem 3.9. *The DFE E_0 of Model (2.1) is locally asymptotically stable if $\mathcal{R}_0 < 1$, and unstable if $\mathcal{R}_0 > 1$.*

Proof. To analyze the local stability of the DFE, we first reduce the dimension of the system using the conservation relations $S_N + I_N + R_N = N$ and $S_B + I_B + R_B = B$, along with $N + B = 1$. Eliminating the recovered compartments yields a five-dimensional system in the variables (N, I_N, I_B, S_N, S_B):

$$\begin{aligned}
\frac{\mathrm{d}N}{\mathrm{d}t} &= -\omega N + \alpha(1 - N),\\
\frac{\mathrm{d}I_N}{\mathrm{d}t} &= \lambda S_N - \gamma_a I_N - \frac{\gamma_t m I_N}{1 + I_N} - \omega I_N + \alpha I_B,\\
\frac{\mathrm{d}I_B}{\mathrm{d}t} &= q\lambda S_B - \gamma_a I_B - \frac{\gamma_t(M - m)I_B}{1 + I_B} + \omega I_N - \alpha I_B,\\
\frac{\mathrm{d}S_N}{\mathrm{d}t} &= -\lambda S_N + \nu(N - S_N - I_N) - \omega S_N + \alpha S_B,\\
\frac{\mathrm{d}S_B}{\mathrm{d}t} &= -q\lambda S_B + \nu(1 - N - S_B - I_B) + \omega S_N - \alpha S_B,
\end{aligned} \tag{3.9}$$

where $\lambda = \beta(I_N + \sigma I_B)$, $\omega = \rho_1(\omega_1(1 - N) + \omega_2(I_N + I_B) + \omega_3)$, and $\alpha = \rho_2(\alpha_1 N + \alpha_2)$.

At the DFE $E_0 = (N^*, 0, 0, S_N^*, S_B^*)$, we have $S_N^* = N^*$, $S_B^* = B^* = 1 - N^*$, and the behavioral rates simplify to $\omega_0 = \rho_1(\omega_1 B^* + \omega_3)$ and $\alpha_0 = \rho_2(\alpha_1 N^* + \alpha_2)$.

The Jacobian matrix of Model (3.9) evaluated at E_0 is

$$J(E_0) = \begin{pmatrix}
\rho_1\omega_1 N^* - \omega_0 + \rho_2\alpha_1 B^* - \alpha_0 & -\rho_1\omega_2 N^* & -\rho_1\omega_2 N^* & 0 & 0\\
0 & \beta N^* - \gamma_a - \gamma_t m - \omega_0 & \beta\sigma N^* + \alpha_0 & 0 & 0\\
0 & q\beta B^* + \omega_0 & q\beta\sigma B^* - \gamma_a - \gamma_t(M - m) - \alpha_0 & 0 & 0\\
\rho_1\omega_1 N^* + \rho_2\alpha_1 B^* + \nu & -\beta N^* - \rho_1\omega_2 N^* - \nu & -\beta\sigma N^* - \rho_1\omega_2 N^* & -\omega_0 - \nu & \alpha_0\\
-\rho_1\omega_1 N^* - \rho_2\alpha_1 B^* - \nu & -q\beta B^* + \rho_1\omega_2 N^* & -q\beta\sigma B^* + \rho_1\omega_2 N^* - \nu & \omega_0 & -\alpha_0 - \nu
\end{pmatrix}.$$

To determine the local stability of the DFE, we compute the eigenvalues of $J(E_0)$. Let l denote an eigenvalue and I_5 the 5×5 identity matrix. The characteristic polynomial is given by $\det(J(E_0) - lI_5)$. Through block decomposition and row/column operations, it can be factored as

$$\begin{aligned}\det\left(J(E_0) - lI_5\right) = &\left(\alpha_0 + \omega_0 + \nu + l\right)\left(\rho_1\omega_1 N^* - \omega_0 + \rho_2\alpha_1 B^* - \alpha_0 - l\right)(\nu + l) \\ &\times \det\begin{pmatrix} \beta N^* - \gamma_a - \gamma_t m - \omega_0 - l & \beta\sigma N^* + \alpha_0 \\ q\beta B^* + \omega_0 & q\beta\sigma B^* - \gamma_a - \gamma_t(M-m) - \alpha_0 - l \end{pmatrix}.\end{aligned}$$

From this factorization, we immediately identify three eigenvalues:

$$\begin{aligned} l_1 &= -\alpha_0 - \omega_0 - \nu < 0, \\ l_2 &= \rho_1\omega_1 N^* - \omega_0 + \rho_2\alpha_1 B^* - \alpha_0 < 0, \\ l_3 &= -\nu < 0. \end{aligned}$$

All of these are real. The eigenvalue l_1 is negative because $\alpha_0, \omega_0, \nu > 0$. The eigenvalue l_3 is negative as $\nu > 0$. We now demonstrate that $l_2 < 0$. At the disease-free equilibrium, the behavioral dynamics satisfy the steady-state equation

$$\dot{N} = G(N) = (\rho_1\omega_1 - \rho_2\alpha_1)N^2 + (-\rho_1\omega_1 - \rho_1\omega_3 + \rho_2\alpha_1 - \rho_2\alpha_2)N + \rho_2\alpha_2 = 0,$$

and the equilibrium value N^* is the unique root of $G(N) = 0$ in the interval $(0, 1)$.

Recall that the eigenvalue associated with the behavioral direction is $l_2 = \rho_1\omega_1 N^* - \omega_0 + \rho_2\alpha_1 B^* - \alpha_0$, where $\omega_0 = \rho_1(\omega_1 B^* + \omega_3)$ and $\alpha_0 = \rho_2(\alpha_1 N^* + \alpha_2)$. A direct computation shows that $l_2 = G'(N^*)$. Now observe the values of $G(N)$ at the boundaries:

$$G(0) = \rho_2\alpha_2 > 0, \qquad G(1) = -\rho_1\omega_3 < 0.$$

Since G is a quadratic polynomial with $G(0) > 0$ and $G(1) < 0$, the unique root N^* in $(0, 1)$ must satisfy $G'(N^*) < 0$. Indeed, if $G'(N^*) \geq 0$, then because $G(N^*) = 0$, the function would be non-decreasing at N^* and hence would remain non-negative for all $N > N^*$; this contradicts $G(1) < 0$. Therefore $G'(N^*) < 0$, and by $l_2 = G'(N^*)$, we obtain $l_2 < 0$.

Thus all three eigenvalues obtained directly from the factorization are negative:

$$l_1 = -\alpha_0 - \omega_0 - \nu < 0, \quad l_2 = G'(N^*) < 0, \quad l_3 = -\nu < 0.$$

The remaining two eigenvalues are those of the 2×2 submatrix

$$J_1 = \begin{pmatrix} \beta N^* - \gamma_a - \gamma_t m - \omega_0 & \beta\sigma N^* + \alpha_0 \\ q\beta B^* + \omega_0 & q\beta\sigma B^* - \gamma_a - \gamma_t(M-m) - \alpha_0 \end{pmatrix}.$$

By the Routh-Hurwitz criterion, both eigenvalues have negative real parts if and only if $\mathrm{tr}(J_1) < 0$ and $\det(J_1) > 0$. After simplification, these conditions are equivalent to $\mathcal{R}_0 < 1$, where $\mathcal{R}_0$ is the basic reproduction number. Therefore, the DFE is locally asymptotically stable when $\mathcal{R}_0 < 1$, and unstable when $\mathcal{R}_0 > 1$.

4. Numerical simulations

To validate the theoretical results and explore the system dynamics, we conduct numerical simulations to investigate the interplay between behavioral adaptation and constrained treatment resources in epidemic transmission. The simulations address the following aspects: a comparison of basic reproduction numbers under different behavioral configurations (Section 4.1); the influence of the behavioral regulation parameters ρ_1 and ρ_2 on the final epidemic size, behavioral prevalence, and the basic reproduction number (Section 4.2); the coupling between the disease reproduction number $\mathcal{R}_0^D$ and the behavioral reproduction number $\mathcal{R}_0^B$, and their joint effect on equilibrium infection levels and system-wide thresholds (Section 4.3); the roles of the behavioral adoption parameters ω_1, ω_2 and ω_3 in shaping the epidemic size, reproduction number, and time to elimination (Section 4.4); and an assessment of behavioral intervention efficacy under varying levels of treatment resources (Section 4.5). Collectively, these analyses provide quantitative insights for the design of effective, resource-aware non-pharmaceutical intervention strategies. Unless specified otherwise, other parameters are as detailed in Table 1. A numerical investigation of the existence and stability of the endemic equilibrium for the full mixed system is provided in the Appendix, where time-series simulations confirm convergence to a positive steady state whenever $\mathcal{R}_0 > 1$.

4.1. Comparison of basic reproduction numbers under different behavioral configurations

To quantify the impact of population-level behavioral heterogeneity on epidemic potential, we numerically compare the basic reproduction numbers derived for the non-behavioral system ($\mathcal{R}_{0,1}$), the fully behavioral system ($\mathcal{R}_{0,2}$), and the mixed system ($\mathcal{R}_0$). Figure 2 presents this comparison across a range of transmission rates β under two distinct regimes of the global behavioral regulation parameters (ρ_1, ρ_2).

Under conventional behavioral transition intensities ($\rho_1 = 1, \rho_2 = 1$), Figure 2(a) confirms the hierarchy $\mathcal{R}_{0,1} > \mathcal{R}_0 > \mathcal{R}_{0,2}$. This indicates that the presence of a behavioral subgroup within a mixed population yields an intermediate transmission potential, demonstrating that partial adoption of protective behaviors can lower the overall epidemic risk compared to a scenario of universal non-adoption.

A critical finding emerges when behavioral adoption is severely insufficient. Setting $\rho_1 = 0.01$ while keeping $\rho_2 = 1$ (Figure 2(b)) leads to $\mathcal{R}_0 > \mathcal{R}_{0,1}$ for a substantial range of β. This counter-intuitive result implies that a mixed system with very weak adoption incentives can exhibit a higher transmission risk than a homogeneous population where no protective behaviors are adopted. This may be attributed to behavioral divergence coupled with an inefficient allocation of constrained treatment resources between the two subgroups, highlighting that inadequately promoted interventions risk exacerbating disease spread. Effective intervention must therefore aim for sufficiently high adoption intensity and compliance to reliably lower the basic reproduction number; half-hearted measures may prove counterproductive.

This study introduces an incomplete protection assumption into the behavior-disease coupling model, which more realistically reflects the effectiveness of health behaviors in the real world compared to the idealized complete-protection scenario in Ryan et al. [28]. Our analysis further reveals the mechanism through which behavioral adoption influences the basic reproduction number. We find that when behavioral adoption is insufficient or protection efficacy is limited, the coupled system's

$\mathcal{R}_0$ may exceed that of a traditional non-behavioral model. This counterintuitive result highlights a critical warning: half-hearted or weakly implemented interventions can exacerbate transmission. It underscores the necessity of implementing large-scale, high-adherence behavioral measures to effectively suppress an epidemic.

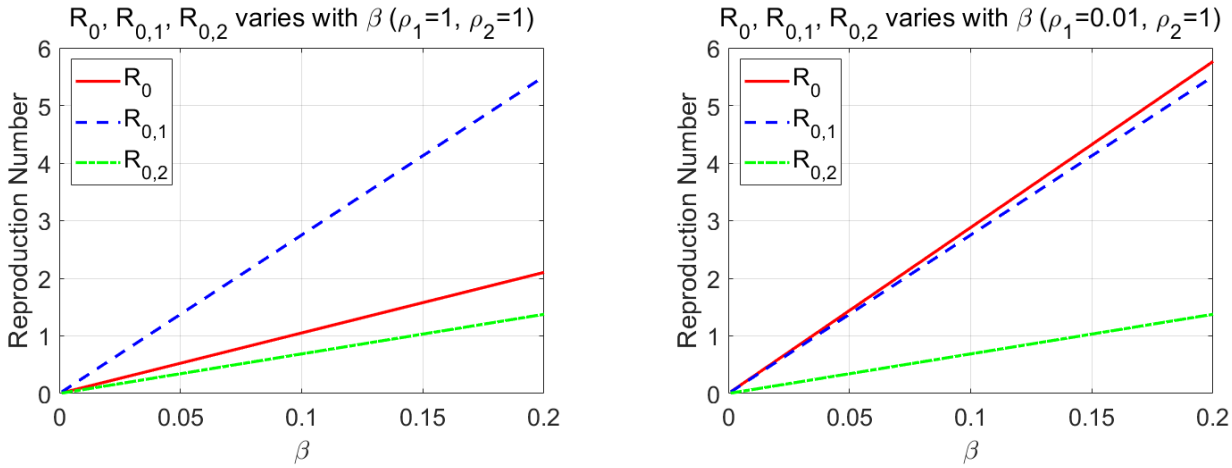

Figure 2. Comparison of basic reproduction numbers under different behavioral configurations. (a) Under balanced transition rates, $\mathcal{R}_0$ lies between $\mathcal{R}_{0,1}$ (non-behavioral) and $\mathcal{R}_{0,2}$ (fully behavioral). (b) When adoption is highly insufficient, $\mathcal{R}_0$ can exceed $\mathcal{R}_{0,1}$. Parameters are as in Table 1. These results demonstrate that partial behavior adoption reduces transmission potential under normal conditions, but insufficient adoption intensity may paradoxically increase epidemic risk compared to no intervention at all.

4.2. Influence of the global modulation parameters for behavioral conversion (ρ_1, ρ_2)

The global parameters ρ_1 and ρ_2 modulate the overall intensity of behavioral adoption and abandonment, respectively. To assess their synergistic effect on epidemic outcomes, we perform a two-parameter sweep while keeping the intrinsic disease reproduction number fixed at $\mathcal{R}_0^D = 3.28$. This value corresponds to a scenario of moderately high transmissibility, representative of many emerging respiratory pathogens. Figure 3 summarizes the results, depicting the final epidemic size, the steady-state proportion of individuals adopting protective behavior (B^*), and the basic reproduction number $\mathcal{R}_0$ of the mixed system.

As shown in Figure 3(a), the final infection size is highly sensitive to both parameters. Increasing ρ_1 (promoting adoption) or decreasing ρ_2 (inhibiting abandonment) substantially reduces the total number of infections. As further illustrated in Figures 3(b),(c), increasing ρ_1 or decreasing ρ_2 significantly elevates the proportion of individuals adopting protective behaviors within the population and drives the system toward a state of universal adoption. This shift in behavioral structure simultaneously induces a systematic reduction in the basic reproduction number $\mathcal{R}_0$. An important finding is that, even when the initial $\mathcal{R}_0 > 1$, synergistically increasing ρ_1 while decreasing ρ_2 can not only substantially reduce the final epidemic scale but may also suppress $\mathcal{R}_0$ below the threshold, thereby achieving theoretical disease elimination. This indicates that under resource-constrained conditions,

effectively intervening in the behavioral transition process enables structural regulation of the epidemic transmission dynamics.

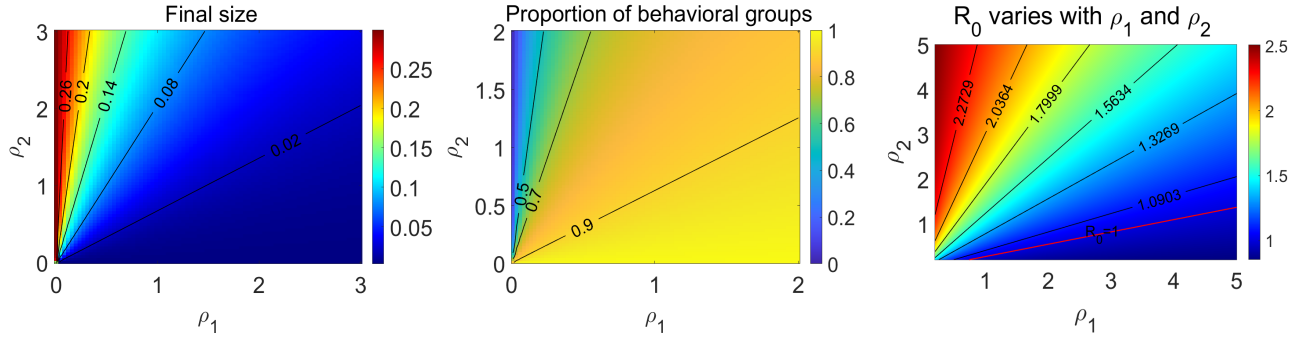

(a) **(b)** **(c)**

Figure 3. Influence of the global behavioral regulation parameters (ρ_1, ρ_2) on epidemic dynamics for a fixed $\mathcal{R}_0^D = 3.28$. (a) Final infection size. (b) Steady-state proportion of individuals adopting protective behavior. (c) Effective basic reproduction number $\mathcal{R}_0$ of the mixed system. The synergistic effect of increasing ρ_1 and decreasing ρ_2 substantially reduces infection burden, elevates behavioral prevalence, and can drive $\mathcal{R}_0$ below the epidemic threshold (the region below the red contour in (c)).

This study quantitatively reveals the synergistic role of the behavioral adjustment parameters ρ_1 and ρ_2 in epidemic control. By enhancing social diffusion, risk perception, and positive incentives (increasing ρ_1) while reducing behavioral fatigue, negative information, and opportunity costs (decreasing ρ_2), the collective behavioral structure can be synergistically optimized, thereby lowering transmission risk. This finding aligns with the research of Agaba et al., though from a distinct perspective: while their work examined how behavioral adoption affects individuals and thereby influences disease spread, the present study directly investigates the impact of behavioral change on transmission dynamics [30]. These results provide a theoretical basis for designing precise and sustainable behavioral intervention strategies, particularly in scenarios with limited treatment resources during emerging infectious disease outbreaks.

4.3. Coupling effects of disease and behavioral reproduction numbers

To elucidate the intrinsic coupling between behavioral dynamics and disease transmission, we analyse the joint regulatory effects of two fundamental threshold parameters: the disease basic reproduction number $\mathcal{R}_0^D$ (intrinsic pathogen transmissibility) and the behavioral reproduction number $\mathcal{R}_0^B$ (self-sustaining diffusion potential of protective behavior). We systematically vary these parameters and examine their combined influence on the steady-state infection scale, the proportion of individuals adopting protective behavior (B^*), and the basic reproduction number ($\mathcal{R}_0$) of the coupled system. Here, $\mathcal{R}_0^B > 1$ indicates that protective behavior possesses autonomous "social contagion" capability.

Figure 4 summarizes the simulation results, revealing a complex yet interpretable interplay. The final infection scale (Figure 4(a)) is primarily driven by $\mathcal{R}_0^D$, as expected. For a fixed $\mathcal{R}_0^B$, reducing $\mathcal{R}_0^D$ is an effective control pathway. However, a key finding is the significant suppressive effect of increasing $\mathcal{R}_0^B$. Notably, when $\mathcal{R}_0^B$ is below 1 and $\mathcal{R}_0^D$ exceeds 1, the final epidemic size remains substantial,

underscoring the challenge of controlling a highly transmissible disease when behavioral adoption lacks self-sustaining momentum. Critically, even for a fixed $\mathcal{R}_0^D$, enhancing $\mathcal{R}_0^B$ by making protective behaviors more "contagious" through social mobilization can independently and substantially reduce infection burden.

The steady-state behavioral adoption proportion (Figure 4(b)) is shaped reciprocally by both thresholds. Holding $\mathcal{R}_0^D$ fixed, variations in $\mathcal{R}_0^B$ (particularly within the range 0–1.5) exert a strong influence on B^*, highlighting the parameter's central role in determining the population's behavioral structure. Conversely, with $\mathcal{R}_0^B$ fixed, an increase in $\mathcal{R}_0^D$ induces a nonlinear rise in adoption, characterized by an initial plateau followed by a sharp increase as the perceived disease threat becomes more salient. The system is especially sensitive when $\mathcal{R}_0^B < 1$, indicating that exogenous interventions (e.g., public campaigns) are crucial to initiate and sustain protective behaviors in the absence of autonomous social diffusion.

The combined effect on the system's basic reproduction number $\mathcal{R}_0$ is shown in Figure 4(c). As anticipated, $\mathcal{R}_0^D$ and $\mathcal{R}_0^B$ have opposing influences: a higher $\mathcal{R}_0^D$ elevates $\mathcal{R}_0$, whereas a higher $\mathcal{R}_0^B$ suppresses it. The contour corresponding to $\mathcal{R}_0 = 1$ delineates the critical boundary for disease elimination. This plot reveals that for a given high $\mathcal{R}_0^D$, a sufficiently high $\mathcal{R}_0^B$ can compensate and drive the coupled system below this threshold, defining a parameter region where "behavioral immunity" can theoretically interrupt transmission. The synergy is most pronounced when enhancing $\mathcal{R}_0^B$ from initially low levels while concurrently managing $\mathcal{R}_0^D$.

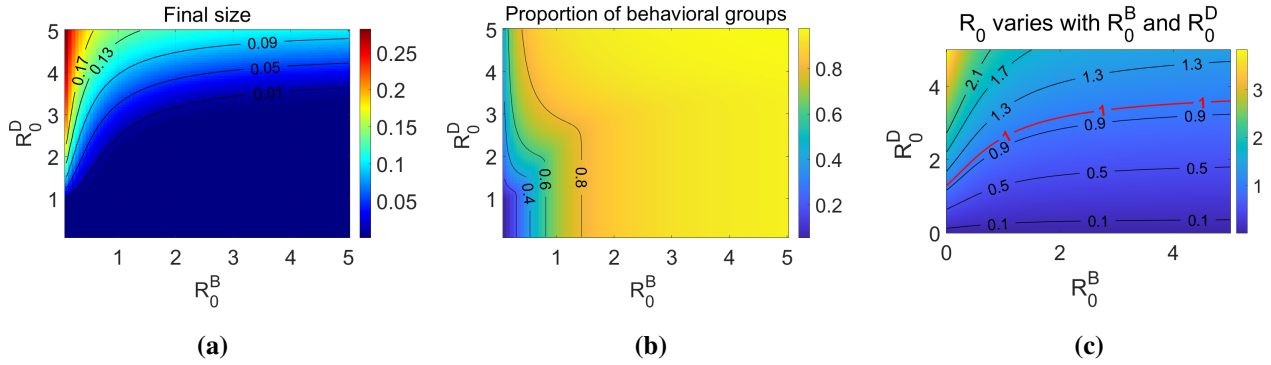

Figure 4. Joint effects of the disease reproduction number $\mathcal{R}_0^D$ and the behavioral reproduction number $\mathcal{R}_0^B$. (a) Final infection size. (b) Steady-state proportion adopting protective behavior. (c) Basic reproduction number $\mathcal{R}_0$ of the coupled system. The $\mathcal{R}_0 = 1$ contour in (c) separates persistent ($\mathcal{R}_0 > 1$) from eliminated ($\mathcal{R}_0 < 1$) regimes. These results demonstrate that a sufficiently high $\mathcal{R}_0^B$ can compensate for high intrinsic pathogen transmissibility, enabling disease elimination even when $\mathcal{R}_0^D > 1$.

Through dual-threshold analysis coupling $\mathcal{R}_0^D$ and $\mathcal{R}_0^B$, this study demonstrates that "behavioral immunity" can function as an intervenable and scalable social defense mechanism. This aligns with the approach of Ryan et al., who similarly examined the dual-threshold coupling of $\mathcal{R}_0^D$ and $\mathcal{R}_0^B$; the numerical simulations here validate their findings [27,28]. In practical epidemic control, efforts should not only target reducing pathogen transmissibility but also focus on reinforcing social norms, elevating public risk awareness and self-efficacy, thereby enabling protective behaviors to acquire autonomous diffusion momentum and fostering sustainable community resilience. This offers a novel theoretical

perspective and quantitative support for designing integrated control strategies in resource-limited or high-transmission-risk scenarios.

4.4. Effects of parameters influencing behavioral adoption

We examine the independent and joint effects of three core behavioral-adoption parameters: social transmission (ω_1), risk-perception response (ω_2), and spontaneous adoption tendency (ω_3), on the final epidemic size and the basic reproduction number $\mathcal{R}_0$. Figure 5 summarizes the simulation results, obtained by varying each parameter individually (Figures 5(a)–(c)), exploring their interactions under three distinct background combinations (Figures 5(d)–(f)), and analysing their influence on $\mathcal{R}_0$ (Figures 5(g)–(i)).

When varied individually, increases in ω_1, ω_2, or ω_3 each reduce the final infection size (Figures 5(a)–(c)), confirming that strengthening any adoption pathway alleviates disease burden. The joint analysis reveals important interactions. Under a low background of the other parameters, increasing ω_1 initially yields only modest reductions, followed by a sharp decline that eventually leads to elimination (Figure 5(d)). This elimination threshold for ω_1 is markedly lower when ω_2 and ω_3 are already at high levels, indicating synergy among adoption drivers. The effect of ω_2 is strongest under a moderate background, where it induces a rapid initial drop in infections (Figure 5(e)). Increases in ω_3 consistently and rapidly reduce infection size, with disease elimination requiring only a modest increment when ω_1 and ω_2 are elevated (Figure 5(f)).

A key mechanistic distinction emerges from the parameters' influence on the system's transmission threshold. Both ω_1 and ω_3 directly lower $\mathcal{R}_0$; when sufficiently large, either can drive $\mathcal{R}_0$ below 1, thereby theoretically interrupting transmission (Figures 5(g),(i)). In contrast, variations in ω_2 have no discernible effect on $\mathcal{R}_0$ (Figure 5(h)), indicating that its protective role operates primarily by accelerating epidemic decline and reducing the final size without altering the fundamental transmission potential.

These findings clarify the complementary functions of the three behavioral drivers. Social transmission (ω_1) and spontaneous tendency (ω_3) act as structural parameters that lower the transmission foundation ($\mathcal{R}_0$) and can enable elimination. Risk-perception response (ω_2) serves as a process parameter that compresses the epidemic curve, making it valuable for rapid outbreak containment even though it does not change $\mathcal{R}_0$. This distinction explains why fear-based campaigns (high ω_2 alone) may curb an ongoing wave but not prevent resurgence without concurrent efforts to strengthen social norms (ω_1) or habitual adoption (ω_3).

Our continuous parameter-variation approach extends the work of [28], who analysed fixed parameter sets. By mapping the full response curves, we identify critical intervals where increases in ω_1 or ω_3 yield the greatest reductions in both final size and $\mathcal{R}_0$. This provides a quantitative basis for staged interventions: in acute phases, emphasizing risk communication (ω_2) can rapidly reduce incidence; for sustained control and elimination, the focus should shift to cultivating self-reinforcing social norms (ω_1) and environments that foster habitual protection (ω_3).

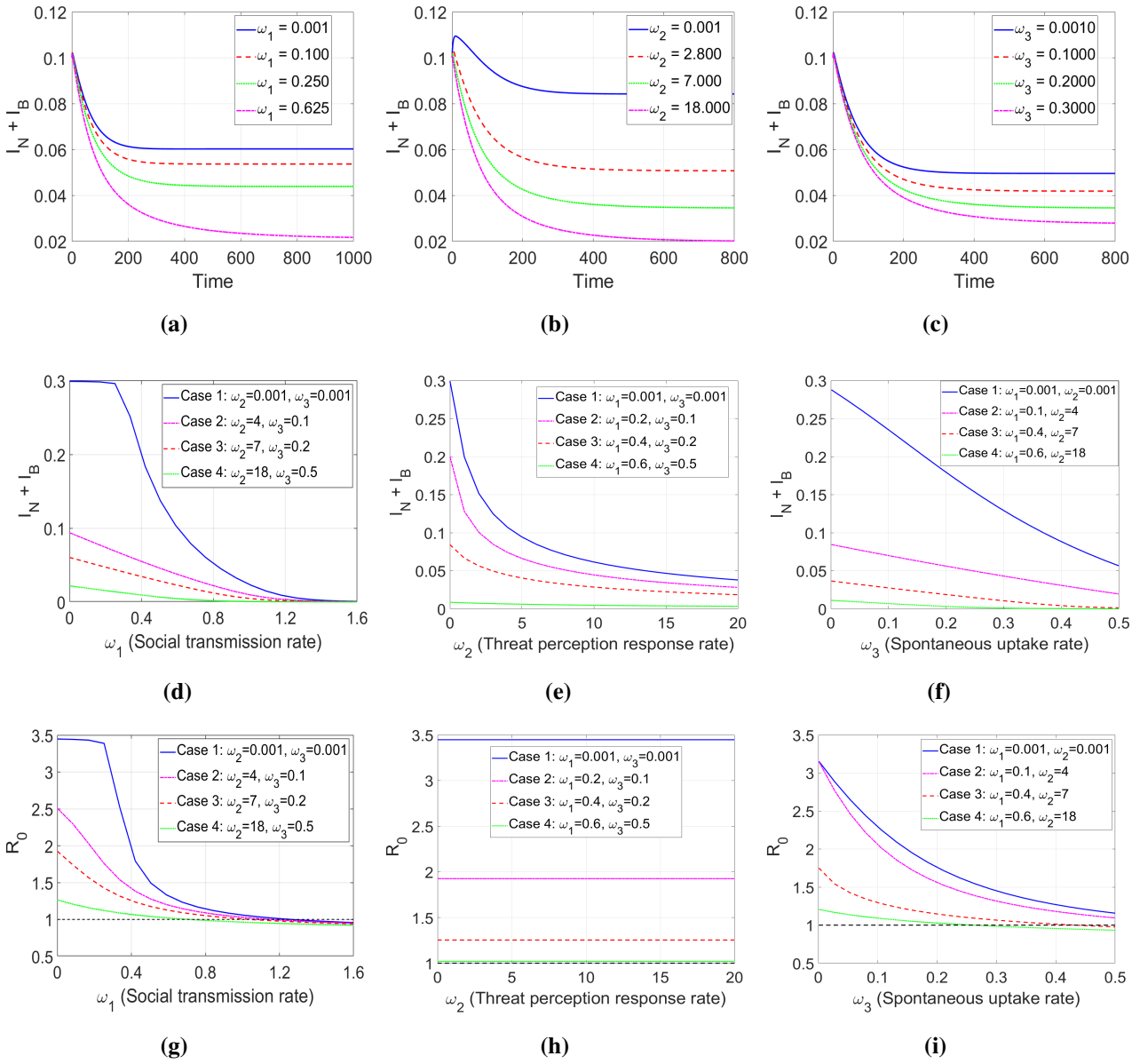

Figure 5. Individual and combined effects of behavioral adoption parameters (ω_1, ω_2, ω_3) on epidemic outcomes. (a)–(c) Final infection size as a function of each parameter independently. (d)–(f) Joint impact on infection size under three distinct parameter-background combinations. (g)–(i) Corresponding influence on the basic reproduction number $\mathcal{R}_0$, illustrating the threshold condition for disease elimination.

4.5. Control efficacy under resource constraints and varying behavioral intensity

We examine how the availability of treatment resources, quantified by the maximum capacity M, interacts with behavioral interventions to shape epidemic outcomes. Simulations are performed for a fixed transmission rate $\beta = 0.2$ under three behavioral-regulation scenarios: a baseline ($\rho_1 = \rho_2 = 1$), a high-abandonment scenario ($\rho_1 = 1, \rho_2 = 2$), and a high-adoption scenario ($\rho_1 = 2, \rho_2 = 1$). The effects on final infection size, basic reproduction number $\mathcal{R}_0$, and disease extinction time ($\nu = 0$) are

shown in Figure 6.

As expected, increasing treatment resources M reduces both the final infection size and $\mathcal{R}_0$ across all behavioral scenarios (Figures 6(a),(b)), confirming that expanding medical capacity directly suppresses transmission. A more nuanced picture emerges for the time to disease elimination (Figure 6(c)). Under the baseline and high-adoption scenarios, raising M shortens the elimination time. In contrast, under the high-abandonment scenario, increasing M paradoxically prolongs the time to elimination. This counterintuitive result suggests that when behavioral adoption is weak and abandonment is high, simply adding treatment resources may extend the epidemic's tail rather than hasten its end.

The findings highlight a critical interaction between resource investment and behavioral sustainability. Enhancing treatment capacity is most effective when accompanied by strong, sustained behavioral adoption. If behavioral promotion is insufficient, increased resources alone may not improve and could even worsen the timeliness of control. Public-health strategies should therefore aim for synergy: expanding medical resources must be coupled with efforts to maintain high adoption rates and minimize abandonment. Such an integrated approach ensures that resource investments simultaneously reduce epidemic scale and accelerate its decline, offering a practical framework for balancing "resource expansion" with "behavioral maintenance" in resource-limited outbreak settings.

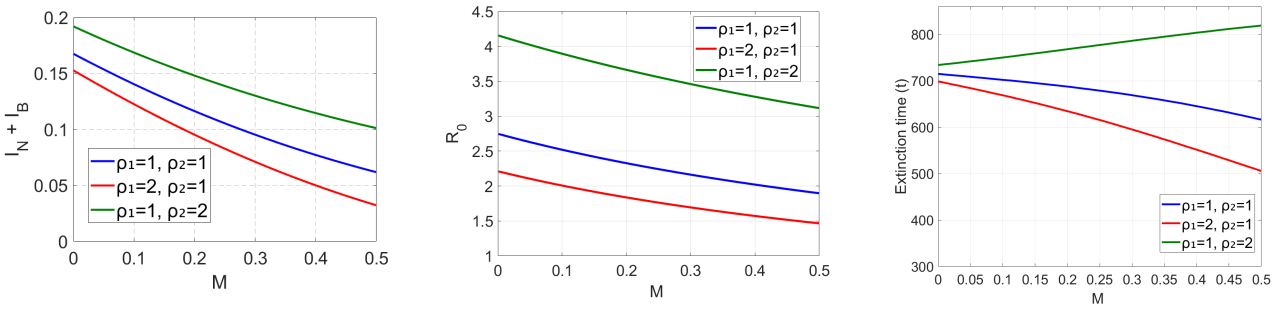

(a) Final infection size **(b)** $\mathcal{R}_0$ **(c)** Time to elimination

Figure 6. Control efficacy under varying treatment resource M and three behavioral scenarios: baseline ($\rho_1 = \rho_2 = 1$), high abandonment ($\rho_1 = 1, \rho_2 = 2$), and high adoption ($\rho_1 = 2, \rho_2 = 1$). (a) Final infection size, (b) basic reproduction number, and (c) disease extinction time (let $\nu = 0$).

5. Conclusions and discussion

Emerging infectious disease outbreaks are characterized by a tight coupling between individual protective behaviors and constrained treatment resources, both of which critically shape transmission trajectories and intervention outcomes. To investigate their synergistic effects, this study developed an epidemic dynamics model that integrates heterogeneous behavioral transitions and treatment-resource saturation within a unified framework. Through theoretical analysis and systematic numerical simulations, we examined how population-level behavioral adaptation under resource-limited conditions modulates the epidemic threshold, final scale, and time to elimination.

The theoretical analysis established dynamical frameworks for three systems: no-behavior adoption, full-behavior adoption, and a mixed population. For each, we derived the basic reproduction number $\mathcal{R}_0$ and analysed equilibrium existence and stability. The results confirm that protective behaviors elevate

the epidemic threshold by reducing both susceptibility and infectiousness. A key theoretical insight is that when behavioral adoption is insufficient (e.g., very small ρ_1), the mixed system can exhibit a higher transmission risk than a system with no adoption at all (Figure 2(b)). This counter-intuitive possibility extends the findings of [27,28] and highlights that poorly implemented behavioral interventions can be counterproductive.

Numerical simulations further reveal the nuanced interplay between behavior and resources. Increasing the global adoption-intensity parameter ρ_1 or decreasing the abandonment parameter ρ_2 elevates the protective-behavior prevalence, reduces the final infection size, and can suppress $\mathcal{R}_0$ below the critical threshold even under resource constraints, enabling theoretical disease elimination (Figure 3). The analysis also demonstrates a coupled regulatory mechanism between the disease and behavioral reproduction numbers ($\mathcal{R}_0^D$ and $\mathcal{R}_0^B$): even for a pathogen with high intrinsic transmissibility, enhancing the social transmissibility of protective behaviors (raising $\mathcal{R}_0^B$) can significantly suppress epidemic spread (Figure 4). This finding validates and quantitatively elaborates the dual-threshold framework proposed by [28]. Furthermore, the core behavioral drivers—social transmission (ω_1), risk-perception response (ω_2), and spontaneous adoption (ω_3)—play distinct, complementary roles: ω_1 and ω_3 directly lower the transmission threshold ($\mathcal{R}_0$), while ω_2 accelerates epidemic decline without altering $\mathcal{R}_0$ (Figure 5). Importantly, under limited resources, merely expanding treatment capacity may prolong the time to elimination if behavioral adoption is weak and abandonment is high, underscoring the necessity of synergizing "resource expansion" with "behavioral maintenance".

In contrast to prior studies that often examine behavior or resources in isolation [30], the principal contribution of this work is the integrated dynamical coupling of behavioral transitions and resource saturation. By introducing the adjustable global parameters ρ_1 and ρ_2, the model provides a quantitative tool for assessing how behavioral interventions can optimize control under resource constraints. The results demonstrate that in resource-limited settings, actively promoting and sustaining protective behaviors constitutes a powerful non-pharmaceutical strategy, capable of reducing the infection peak, shrinking the epidemic scale, and potentially interrupting transmission chains.

These findings offer concrete guidance for public health policy. Behavioral advocacy should be initiated early and sustained to strengthen social diffusion (ω_1) and the foundation for spontaneous adoption (ω_3), thereby lowering the system-wide transmission threshold. When treatment resources are strained, policymakers must ensure behavioral interventions achieve sufficient intensity and coverage to avoid unintended increases in transmission risk. Resource allocation should be designed synergistically: expanding medical capacity must be accompanied by campaigns and incentives that maintain high adoption rates and low abandonment, ensuring investments reduce both the scale and duration of the epidemic.

Several limitations of this study point to fruitful directions for future research. First, behavioral transition rates are assumed independent of an individual's infection status; future models could incorporate how being infected, symptomatic, or recovered differentially influences behavioral choices. Second, the model does not distinguish between symptomatic and asymptomatic infected individuals, who may differ in both behavior and treatment access; incorporating such heterogeneity [37,38] would enhance realism. Finally, the present framework can be integrated with other interventions—such as testing, isolation, and vaccination—to form a comprehensive multi-strategy assessment tool, providing stronger theoretical support for managing complex epidemics.

In summary, by constructing a coupled "behavior–resource–disease" dynamic model, this

study quantitatively reveals the critical, nonlinear role of behavioral transitions under constrained treatment resources. It provides a mathematical foundation and a decision-making reference for designing precise, sustainable, and integrated non-pharmaceutical intervention strategies in resource-limited settings.

Use of AI tools declaration

The authors declare they have not used Artificial Intelligence (AI) tools in the creation of this article.

Acknowledgments

This research is supported by the National Natural Science Foundation of China (No. 12271401, W2421101) and the Natural Science Foundation of Tianjin, China (No. 22JCYBJC00080).

Conflict of interest

The authors declare there are no conflicts of interest.

References

1. D. M. Morens, G. K. Folkers, A. S. Fauci, The challenge of emerging and re-emerging infectious diseases, *Nature*, **430** (2004), 242–249. https://doi.org/10.1038/nature02759
2. K. E. Jones, N. G. Patel, M. A. Levy, A. Storeygard, D. Balk, J. L. Gittleman, et al., Global trends in emerging infectious diseases, *Nature*, **451** (2008), 990–993. https://doi.org/10.1038/nature06536
3. N. Wang, L. Qi, M. Bessane, M. Hao, Global Hopf bifurcation of a two-delay epidemic model with media coverage and asymptomatic infection, *J. Differ. Equations*, **369** (2023), 1–40. https://doi.org/10.1016/j.jde.2023.05.036
4. N. Wang, L. Qi, G. Cheng, Dynamical analysis for the impact of asymptomatic infective and infection delay on disease transmission, *Math. Comput. Simul.*, **200** (2022), 525–556. https://doi.org/10.1016/j.matcom.2022.04.029
5. P. P. Win, Z. Lin, M. Zhang, The final size and critical times of an SIVR epidemic model, *Adv. Contin. Discrete Models*, **2025** (2025), 31. https://doi.org/10.1186/s13662-025-03902-2
6. M. Jusup, P. Holme, K. Kanazawa, M. Takayasu, I. Romić, Z. Wang, et al., Social physics, *Phys. Rep.*, **948** (2022), 1–148. https://doi.org/10.1016/j.physrep.2021.10.005
7. Y. Li, Y. Yao, M. Feng, T. P. Benko, M. Perc, J. Završnik, Epidemic dynamics in homes and destinations under recurrent mobility patterns, *Chaos, Solitons Fractals*, **195** (2025), 116273. https://doi.org/10.1016/j.chaos.2025.116273
8. W. Wu, Q. Zhang, H. Wang, S. Liu, Cholera dynamics driven by human behavior change via a degenerate reaction-diffusion model, *Z. Angew. Math. Phys.*, **76** (2025), 114. https://doi.org/10.1007/s00033-025-02495-w

9. M. Ryan, E. Brindal, R. I. Hickson, Behavior and infection feedback loops inform early-stage behavior emergence and the efficacy of interventions, *Math. Med. Life Sci.*, **2** (2025), 2452444. https://doi.org/10.1080/29937574.2025.2452444
10. G. Fan, J. Li, J. Belair, H. Zhu, Delayed model for the transmission and control of COVID-19 with Fangcang shelter hospitals, *SIAM J. Appl. Math.*, **83** (2023), 276–301. https://doi.org/10.1137/21M146154X
11. S. Gao, P. Binod, C. W. Chukwu, T. Kwofie, S. Safdar, L. Newman, et al., A mathematical model to assess the impact of testing and isolation compliance on the transmission of COVID-19, *Infect. Dis. Modell.*, **8** (2023), 427–444. https://doi.org/10.1016/j.idm.2023.04.005
12. I. Ahmad, H. Seno, An epidemic dynamics model with limited isolation capacity, *Theory Biosci.*, **142** (2023), 259–273. https://doi.org/10.1007/s12064-023-00399-9
13. Z. Fu, H. Seno, SIRI+Q model with a limited capacity of isolation, *Theory Biosci.*, **144** (2025), 121–144. https://doi.org/10.1007/s12064-025-00437-8
14. H. Zhao, L. Wang, S. M. Oliva, H. Zhu, Modeling and dynamics analysis of Zika transmission with limited medical resources, *Bull. Math. Biol.*, **82** (2020), 99. https://doi.org/10.1007/s11538-020-00776-1
15. J. Wang, S. Liu, B. Zheng, Y. Takeuchi, Qualitative and bifurcation analysis using an SIR model with a saturated treatment function, *Math. Comput. Modell.*, **55** (2012), 710–722. https://doi.org/10.1016/j.mcm.2011.08.045
16. B. Tang, W. Zhou, X. Wang, H. Wu, Y. Xiao, Controlling multiple COVID-19 epidemic waves: an insight from a multi-scale model linking the behavior change dynamics to the disease transmission dynamics, *Bull. Math. Biol.*, **84** (2022), 106. https://doi.org/10.1007/s11538-022-01061-z
17. A. D. Becker, K. H. Grantz, S. T. Hegde, S. Bérubé, D. A. T. Cummings, A. Wesolowski, Development and dissemination of infectious disease dynamic transmission models during the COVID-19 pandemic: what can we learn from other pathogens and how can we move forward?, *Lancet Digit. Health*, **3** (2021), e41–e50. https://doi.org/10.1016/S2589-7500(20)30268-5
18. J. Bedson, L. A. Skrip, D. Pedi, S. Abramowitz, S. Carter, M. F. Jalloh, et al., A review and agenda for integrated disease models including social and behavioral factors, *Nat. Hum. Behav.*, **5** (2021), 834–846. https://doi.org/10.1038/s41562-021-01136-2
19. S. Funk, S. Bansal, C. T. Bauch, K. T. D. Eames, W. J. Edmunds, A. P. Galvani, et al., Nine challenges in incorporating the dynamics of behavior in infectious diseases models, *Epidemics*, **10** (2015), 21–25. https://doi.org/10.1016/j.epidem.2014.12.005
20. R. N. Shalan, R. Shireen, A. H. Lafta, Discrete an SIS model with immigrants and treatment, *J. Interdiscip. Math.*, **24** (2020), 1201–1206. https://doi.org/10.1080/09720502.2020.1814496
21. W. O. Kermack, A. G. McKendrick, A contribution to the mathematical theory of epidemics, *Proc. R. Soc. A*, **115** (1927), 700–721. https://doi.org/10.1098/rspa.1927.0118
22. D. P. Durham, E. A. Casman, Incorporating individual health-protective decisions into disease transmission models: a mathematical framework, *J. R. Soc. Interface*, **9** (2012), 562–570. https://doi.org/10.1098/rsif.2011.0325

23. C. J. Fan, Y. Jin, L. A. Huo, C. Liu, Y. P. Yang, Y. Q. Wang, Effect of individual behavior on the interplay between awareness and disease spreading in multiplex networks, *Physica A*, **461** (2016), 523–530. https://doi.org/10.1016/j.physa.2016.06.050

24. L. Hébert-Dufresne, D. Mistry, B. M. Althouse, Spread of infectious disease and social awareness as parasitic contagions on clustered networks, *Phys. Rev. Res.*, **2** (2020), 033306. https://doi.org/10.1103/PhysRevResearch.2.033306

25. N. Perra, D. Balcan, B. Gonçalves, A. Vespignani, Towards a characterization of behavior-disease models, *PLoS One*, **6** (2011), e23084. https://doi.org/10.1371/journal.pone.0023084

26. J. M. Epstein, E. Hatna, J. Crodelle, Triple contagion: a two-fears epidemic model, *J. R. Soc. Interface*, **18** (2021), 20210186. https://doi.org/10.1098/rsif.2021.0186

27. M. Ryan, E. Brindal, M. Roberts, R. I. Hickson, A behavior and disease transmission model: incorporating the Health Belief Model for human behavior into a simple transmission model, *J. R. Soc. Interface*, **21** (2024), 20240038. https://doi.org/10.1098/rsif.2024.0038

28. M. Ryan, R. I. Hickson, E. M. Hill, T. House, V. Isham, D. Zhang, et al., A behavior and disease model of testing and isolation, preprint, arXiv:2504.02488.

29. A. Kaur, R. C. Tyson, I. R. Moyles, The impact of fear and behavior response to established and novel diseases, *SIAM J. Appl. Math.*, **85** (2025), 687–710. https://doi.org/10.1137/24M1670718

30. G. O. Agaba, Y. N. Kyrychko, K. B. Blyuss, Mathematical model for the impact of awareness on the dynamics of infectious diseases, *Math. Biosci.*, **286** (2017), 22–30. https://doi.org/10.1016/j.mbs.2017.01.009

31. Y. Shang, Global stability of disease-free equilibria in a two-group SI model with feedback control, *Nonlinear Anal. Model. Control*, **20** (2015), 501–508. https://doi.org/10.15388/NA.2015.4.3

32. P. Van den Driessche, Reproduction numbers of infectious disease models, *Infect. Dis. Modell.*, **2** (2017), 288–303. https://doi.org/10.1016/j.idm.2017.06.002

33. O. Diekmann, J. A. P. Heesterbeek, J. A. J. Metz, On the definition and the computation of the basic reproduction ratio R_0 in models for infectious diseases in heterogeneous populations, *J. Math. Biol.*, **28** (1990), 365–382. https://doi.org/10.1007/BF00178324

34. Y. Bai, X. Wang, S. Guo, Global stability of a mumps transmission model with quarantine measure, *Acta Math. Appl. Sin.*, **37** (2021), 665–672. https://doi.org/10.1007/s10255-021-1035-7

35. S. Guo, Y. Xue, M. He, J. Cui, Modeling and analysis of malaria transmission dynamics considering vaccination and vaccine failure, *Acta Math. Appl. Sin.*, **47** (2024), 1–11. https://doi.org/10.20142/j.cnki.amas.202401001

36. J. P. LaSalle, *The Stability of Dynamical Systems*, SIAM, 1976. https://doi.org/10.1137/1.9781611970432

37. M. Shen, Y. Xiao, G. Zhuang, Y. Li, L. Zhang, Mass testing–An underexplored strategy for COVID-19 control, *Innovation*, **2** (2021), 100114. https://doi.org/10.1016/j.xinn.2021.100114

38. D. P. Oran, E. J. Topol, Prevalence of asymptomatic SARS-CoV-2 infection: a narrative review, *Ann. Intern. Med.*, **173** (2020), 362–367. https://doi.org/10.7326/M20-3012

Appendix

Existence of the endemic equilibrium

Owing to the high dimensionality and nonlinear coupling in the full mixed system (2.1), an analytical characterization of the endemic equilibrium is infeasible. We therefore resort to numerical simulations to verify the existence and stability of the endemic state when the coupled reproduction number exceeds unity.

Figure A1 displays the time evolution of all compartments for a parameter set satisfying $\mathcal{R}_0 > 1$ (e.g., $\beta = 0.2$, with the other parameters as in Table 1). Both infected populations converge to positive steady states, confirming that a unique endemic equilibrium exists and is locally asymptotically stable whenever $\mathcal{R}_0 > 1$.

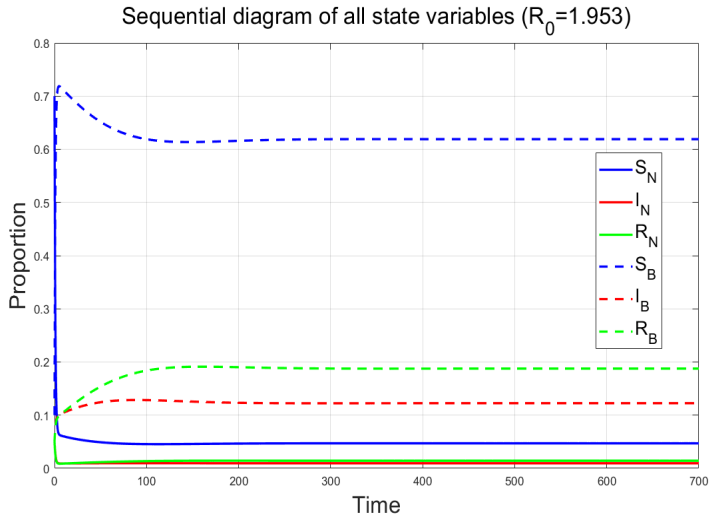

Figure A1. Time series of all compartments for Model (2.1) with $\mathcal{R}_0 > 1$. Parameters are as in Table 1 with $\beta = 0.2$ and $\rho_1 = \rho_2 = 1$. Both infected populations converge to positive steady states, illustrating the existence of a stable endemic equilibrium when the disease invades.